Development of a Wind Turbine Test Rig and Rotor for Trailing Edge Flap Investigation: Static Flap Angles Case

Ahmed Abdelrahman[1] **and David A. Johnson**
Department of Mechanical Engineering, University of Waterloo, Waterloo, ON, N2L 3G1, Canada

E-mail: a5abdelr@uwaterloo.ca, da3johns@uwaterloo.ca

Abstract. One of the strategies used to improve performance and increase the life-span of wind turbines is active flow control. It involves the modification of the aerodynamic characteristics of a wind turbine blade by means of moveable aerodynamic control surfaces. Trailing edge flaps are relatively small moveable control surfaces placed at the trailing edge of a blade's airfoil that modify the lift of a blade or airfoil section. An instrumented wind turbine test rig and rotor were specifically developed to enable a wide-range of experiments to investigate the potential of trailing edge flaps as an active control technique. A modular blade based on the S833 airfoil was designed to allow accurate instrumentation and customizable settings. The blade is 1.7 meters long, had a constant 178mm chord and a 6° pitch. The modular aerodynamic parts were 3D printed using plastic PC-ABS material. The blade design point was within the range of wind velocities in the available large test facility. The wind facility is a large open jet wind tunnel with a maximum velocity of 11m/s in the test area. The capability of the developed system was demonstrated through an initial study of the effect of stationary trailing edge flaps on blade load and performance. The investigation focused on measuring the changes in flapwise bending moment and power production for different trailing edge flap spanwise locations and deflection angles. The relationship between the load reduction and deflection angle was linear as expected from theory and the highest reduction was caused by the flap furthest from the rotor center. Overall, the experimental setup proved to be effective in measuring small changes in flapwise bending moment within the wind turbine blade and will provide insight when (active) flap control is targeted.

1. Introduction

Wind turbine research focuses on building more efficient and more economic wind turbines. This resulted in larger rotors being built and more sophisticated technologies being applied in operating modern wind turbines. One of the strategies to improve performance and life-span of wind turbines is active flow control. Active flow control involves the modification of the aerodynamic characteristics of a wind turbine blade by means of moveable aerodynamic control surfaces. The aerodynamic control surface can be the full blade, segments of it or smaller more distributed surfaces along the blade such as micro tabs and flaps [1]. Recently, research has focused on blades that incorporate distributed and embedded intelligent systems of sensors and actuators. Such technology is referred to as 'smart rotors' [2]. Active trailing edge flaps (TEFs) are one of the methods proposed in designing a smart rotor. TEFs are relatively small moveable control surfaces that alter the airfoil camber line resulting in lift

[1] To whom any correspondence should be addressed.

alteration. The ultimate goal of the technology is to reduce the effect of freestream wind fluctuations on the blade load.

These moveable surfaces can achieve significantly high changes in the lift coefficient of the sections they alter in response to their small deflections [3]. This is an effect of the increase or decrease of the camber of the airfoil of that section based on the side of deployment as shown in Figure 1. The distributed surfaces are usually operated by separate control mechanisms (sensors and actuators) which has several advantages compared to traditional full blade pitch systems. They have better structural and safety features and require less power for activation since they have significantly lower surface inertia than full span pitch control, mainly due to their size [1]. Lower surface inertia is also pivotal to enable high frequency control.

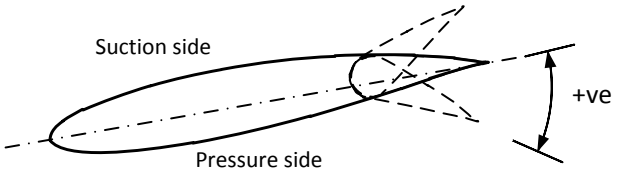

Figure 1. Illustration of hinged TEF on an S833 airfoil.

Wind turbines are subject to extreme fatigue load cycles due to the highly fluctuating nature of the wind resource. Hence, most wind turbine components' design are governed by fatigue instead of ultimate loads [4]. The ability to alleviate such loads would allow a reduction in weight, and increase the size and life-span of blades.

Individual and collective pitch control are one of the traditional and widely used active flow control methods for large wind turbines. Pitch control has proved to significantly reduce fatigue load increments due to relatively low frequency variations on the blade conditions caused by yaw error, wind shear and gusts [5]. Larsen et al. [6] showed that individual pitch control can reduce fatigue loads by 25% and the maximum load on the turbine by 6% when measuring bending moment at the hub. As wind turbines become larger, however, their blades become heavier and more flexible. This adds more stress on pitch bearings and increases the response time between the stimulating input and actuation of the active system.

Smaller more distributed control devices can achieve faster response times and require smaller embedded components. They also showed promising fatigue load reduction potential through a series of computational simulations and experimental studies. Lackner and Kuik [7] investigated the potential of hinged TEFs to reduce fatigue load on the Upwind 5MW reference turbine [8] by simulation. The study utilized GH Bladed, an aero-elastic simulation code, and designed external controllers for the turbine and smart rotor to simulate the effect of applying individual flap control. Applying a flap between 70% and 90% of the blade, they reported reduction between 12% and 15% in the damage equivalent load in the flapwise direction. In a similar study, Andersen *et al.* [9] also reported fatigue load reductions up to 25% applied to a model of the same Upwind reference turbine using deformable TEFs were used rather than the more traditional hinged TEFs. It is not clear how much the use of deformable TEFs contributed to the higher reduction ratio.

In an experimental study, Hulskamp *et al.* [10] designed a two-blade 1.8m diameter rotor that reflects the dynamic behaviour of the Upwind reference [8] turbine using non-dimensional scaling. Strain gages were used to measure the flapwise bending moments. The setup incorporated TEFs that had fixed length and location, hence only one flap setting could be investigated. Significant dynamic load reductions were reported using different controller designs for the activating the TEFs. However, the effect on the power production of the wind turbine was not measured.

Since the potential of flow control using aerodynamic control devices was strongly supported through modelling and experiments and upon the review of related studies, it was found that there was significantly more work done on computational simulations and numerical modelling with solemn experimental validation. The potential contribution of an experimental platform that could investigate the effects of aerodynamic control devices in controlled operating conditions was evident. Focusing on hinged TEFs, an instrumented wind turbine test rig and rotor were developed to enable a wide-range of experimental set-ups for such investigations. The capability of the developed system was demonstrated through a steady state study of the effect of TEFs on blade load and power production.

2. **Effect of TEFs**

TEFs were first developed for airplanes to improve the coefficient of lift (C_l) of wings to increase loading during take-off and landing without changing the characteristics of cruising and high-speed flights [3]. They are categorized as high-lift devices, which also include leading edge slats, slotted-flaps, split flaps and external airfoil flap. Some of the common high-lift devices are illustrated in Figure 2.

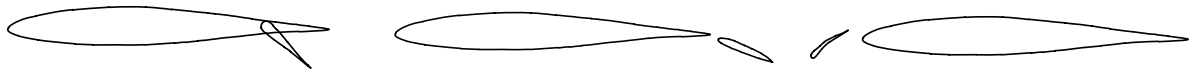

Plain flap* External airfoil flap Leading edge slat

Figure 2. Some typical high-lift devices. Adapted from [3]. **used in this study.*

The device of interest for this study was the plain TEF, also known as an aileron. The plain TEF is formed by hinging a trailing edge section at a point within the contour [3]. Downward deflection of the flap (towards the pressure side) is called a 'positive deflection' and was found to increase the C_l at the current angle of attack (α) and the maximum C_l but also causes it to happen at a lower α. In contrast, an upward deflection decreases the C_l at the current α and the maximum C_l but causes it to happen at a higher α [11].

Deflection of the TEF changes the effective camber of an airfoil resulting in changes to its aerodynamic characteristics. Thin airfoil theory can be used to predict the effect of a plain TEF on the C_l of an airfoil [12]. It shows that the distribution of circulation which creates the lift forces consists of the sum of a component due to α and a component due to the camber for any general airfoil. Thin airfoil theory solution of the distribution of chordwise circulation based on its assumptions for a general airfoil shows that (derivation can be found in [3,12]):

$$C_l = 2\pi\alpha + \pi(A_1 - 2A_0) \quad (1)$$

where A_1 and A_0 are Fourier series constants that are functions of the geometry of the airfoil. The first part of the right hand side, $2\pi\alpha$, accounts for the effect of α, while the second part, $\pi(A_1 - 2A_0)$, accounts for the camber of the original airfoil. The addition of the flap modifies the problem to the case of finding the distribution due to a camber line made up of the chord of the airfoil and the chord of the deflected flap at the flap angle. The influence of a flap deflection can be considered as an addition to both these components [12].vThe new C_l can be shown as (derivation can be found in [3,12]):

$$C_l = 2\pi\alpha + 2(\pi - \phi + \sin\phi)\eta \quad 2)$$

where η is the flap angle, and ϕ is a constant that is a function of the airfoil geometry. The flap load can be obtained using the thin airfoil theory equation with limited accuracy because the effects of viscosity that are particularly prominent over the trailing edge of the airfoil are not accounted for. Also the theory is limited to small angles of attack and can't predict the increase in maximum C_l due to the flap. However, an important conclusion that can be made from these solutions is that, in theory, C_l is linearly changing with the flap deflection angle η.

3. **Experimental Set-up**

3.1. Facility

The facility used for the experiments was an open jet wind tunnel with a relatively large plenum, and the flow was driven by a set of six fans with limited flow conditioning. The flow has relatively high turbulence and a low blockage ratio can be obtained for test subjects. Details about the facility fan specifications and wind tunnel geometry are in Table 1.

Table 1. UW Facility fan specifications [13].

Specification	**Value**	**Details**
Volume Flow rate	78.7 m^3 /s	Maximum x 6 fans
Pressure	413.5 Pa	At maximum flow rate
Fan discharge plenum	8.23 m long, 8.54 m wide, 5.9 m high	
Plenum exit plane	Rectangular 8.0 m wide, 5.9 m high	
Test area	15.4 m wide, 19.5 m long, 7.8 m high at the sides	
Flow exit	Squared, 7.9 m wide, 7.9 m high	

Further details of the geometry and flow analysis of this facility may be found in Devaud *et al.* [13] and Gaunt [14]. This facility in its current configuration is capable of producing nominal wind speeds between 0 and 11.5 m/s with turbulence intensities in the range of 5.9% to 6.2% as reported by Gertz [15].

3.2. Turbine test rig

The apparatus utilized in this study was a specially designed and purpose built wind turbine test rig. The turbine test rig's main function was to control the rotation speed of the rotor and provide power measurements. The motor utilized was capable of acting as a generator based on the output shaft torque supply. It also included an encoder for accurate speed control through a feedback loop with a variable frequency drive. Figure 3 shows the different components of the nacelle. The final specifications of the assembled test rig are listed in Table 2.

Table 2. Final test rig specifications

Specification	**Value/Range**	**Details**
rotation speed	0-230	rpm
yaw angle	± 20	degrees
power capacity	3.7	kW

3.3. Rotor and 3D Printed Blade

A single bladed rotor was designed and fabricated for this study. The rotor consisted of one aerodynamic blade and two cylindrical counterweights that were used for the sole purpose of balancing the rotor to reduce excess vibrations and loads on the hub, bearings and the tower.

3.3.1. Aerodynamic Blade Design.

The primary interest of this study was focused on the changes caused by the TEF activation, thus maximizing blade efficiency through chord and twist optimization was not a priority. A constant chord and twist blade was designed. To maximize the load and power production from such blade, the rotation speed was set near the top of the available range at 200 rpm. The design wind speed was set to 8.5m/s to avoid stall of the single blade within the wind speed range. The NREL S83X [16] series were designed specifically for wind turbines of 1 to 3 m blade length. The S833 airfoil was selected for the full length of the blade based on a BEM analysis performed using PROPID [17]. Also, the

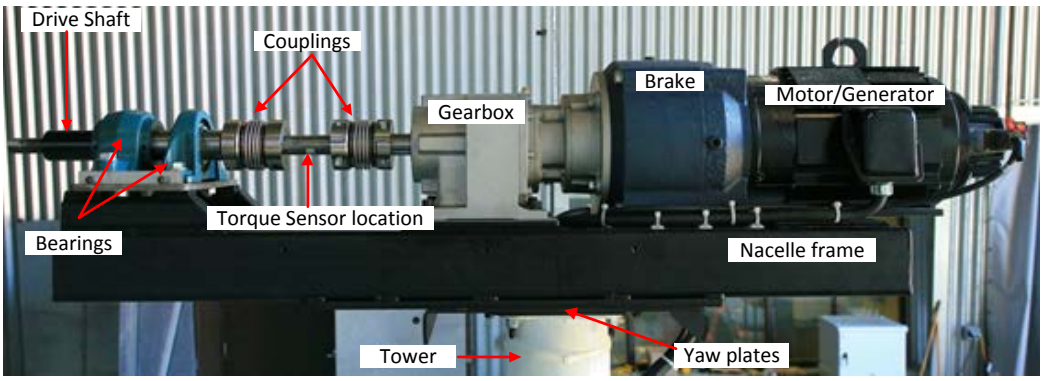

Figure 3. Assembled Nacelle Components (without cover)

airfoil geometry was thick enough near the trailing edge for the flap hinge. The analysis also suggested a chord length of 178 mm and pitch angle of 6° for maximum power production at an 8.5 m/s design and 200 rpm design point for the current configuration. PROPID is a multipoint inverse BEM-based design program for HAWT rotors [17] used for design and off-design blade performance.

3.3.2. Structural Blade Design

The blade was assembled from 3 main components; a tubular spar, hub connection and aerodynamic sections. The tubular spar was the main load bearing component and was placed such that the center of the spar cross section lies on the aerodynamic centre of the airfoil; at one quarter chord from the leading edge. The diameter of the spar was restricted by the thickness of the airfoil at the aerodynamic center. Although the experiments performed in this application were steady state, the blade was designed with future dynamic testing in mind. The dynamic behaviour of the rotor was designed to reflect that of the Upwind 5MW reference turbine [8]. The following equation was used for dynamic scaling [10]:

$$f_{blade} = \frac{f_{ref}\Omega_{blade}}{\Omega_{ref}} \tag{3}$$

where f is the first flapwise bending mode and Ω is the rotation speed. Here f_{blade} was required to be 11 Hz, however, using the largest standard tube capable of fitting internal to the airfoil gave a value of 8.5 Hz. The rotation speed can be reduced to meet the ratio required in equation 3.

The entire aerodynamic part of the blade was 3D printed from a CAD drawing using plastic PC-ABS material. It was made up of five modular sections, two of which contain the TEFs, and a tip section. The five core sections were interchangeable to allow placing the TEFs at different locations along the blade length. The hinged TEFs were capable of a deflection angle within ±25°. A control rod that runs through the blade sections near the trailing edge was used to set the flap angle. The flaps cover 20% of the chord. Figures 4-6 show some blade design details and final assembly.

3.4. Instrumentation and Data Acquisition

3.4.1. Strain Measurement

The blade was instrumented with three strain gage groups located at three positions along its length. The strain gages were placed directly on the steel spar. Each strain gauge group was made up of four strain gages wired in a full-bridge configuration and placed on each side of the spar to measure the out of plane (flapwise) bending moment. Figure 7 shows the strain gage locations relative to the 3D printed blade segments and the distance from the rotor center.

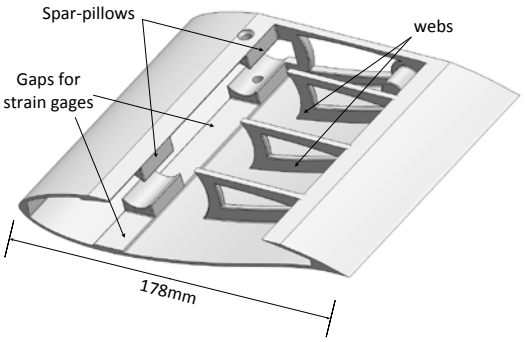

Figure 4. Blade section internal details.

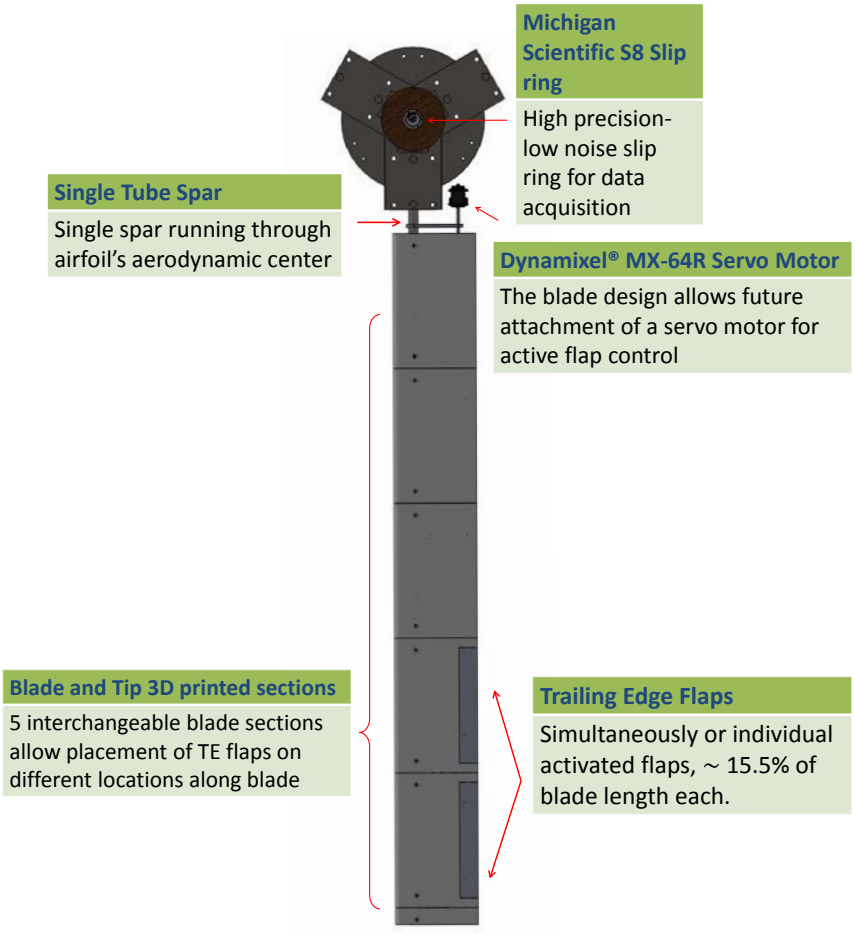

Figure 5. Blade and hub assembly.

Figure 6. Assembled test rig and rotor

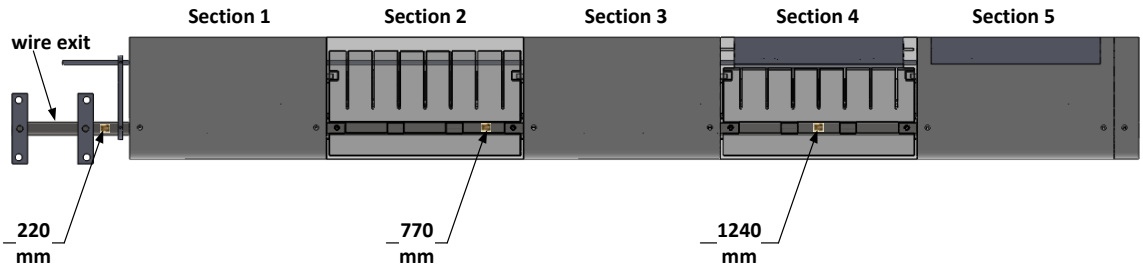

Figure 7. Strain gage group locations (distance indicated from center of the rotor)

3.4.2. Power Measurement
Turbine power production was measured using current and voltage measurements across the dynamic brake resistor. This was automated by the vector drive and feedback rotor speed control system. Table 3 outlines the different measurement points and indicates where power measurements were recorded.

3.4.3. Wind Speed Measurement
Wind speed measurements were obtained using a sonic anemometer (CSAT-3). Using variable frequency drives on the facility fans, 10 fan frequencies were nominally chosen producing wind speeds between 1.5 and 10.5 m/s, with approximately 1 m/s increments, in addition to no wind (0 m/s).

3.4.4. Experimental Procedure and Data Recording
The flap angle was set using a digital protractor measuring the angular location of the control rod. The strain, power and wind speed measurements were logged simultaneously. The sample rate for the strain and power readings were 1 kHz and for the wind speed was 20 Hz. The data averages are reported in this study. The facility wind speed was increased in 1m/s increments for different combinations of flap, location and deflection angles. Figure 8 shows the different flap combinations applied and the configuration code for reference in the results section. Table 3 shows the different measurement points for the flap formations.

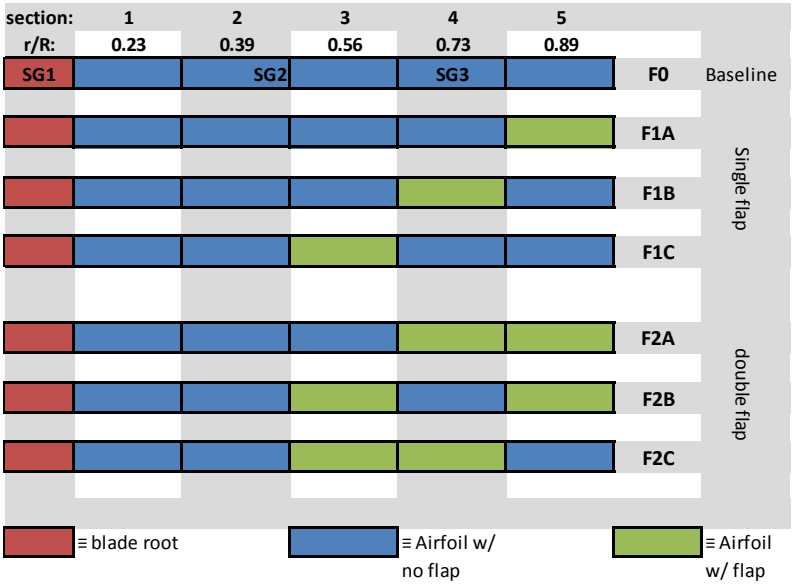

Figure 8. Schematic identifying different flap formations (FXX) and strain gage group (SGX) locations.

Table 3. Measurement Points, *power included for all velocities, ψpower only at design

Flap Formation	Flap Angles (deg)	Wind Speeds (m/s)
F0*	0	0, 1.5-10.5
F1Aψ	-15	0, 1.5-10.5
F1Bψ	-15	0, 1.5-10.5
F1Cψ	-15	0, 1.5-10.5
F2Aψ	-15, -10, -5, 5, 10, 15	0, 1.5-10.5
F2B	(not reported here)	
F2C	(not reported here)	

4. Results

4.1. Baseline Case
The strain gage and power measurements for the baseline case where no flap is activated are used as a reference for comparison with all the flap formations to show the effect of changing the different flap parameters. Power measurement in Figure 9 shows a good correlation with the results predicted by the PROPID model with an increasingly higher prediction beyond 7 m/s. Figure 10 shows the change in moment values with respect to the wind velocity. The trends were increasing with wind speed as expected with higher moments at locations closer to the root. Without the effect of the induction factors, α was calculated at the mid-span of the blade throughout the wind speed range to be almost

linear between -6° at 0 m/s and 25° at 10.5 m/s. Measurement of the induction factors was beyond the scope of this study. In low winds the axial force is negative (C_l was expected to be negative).

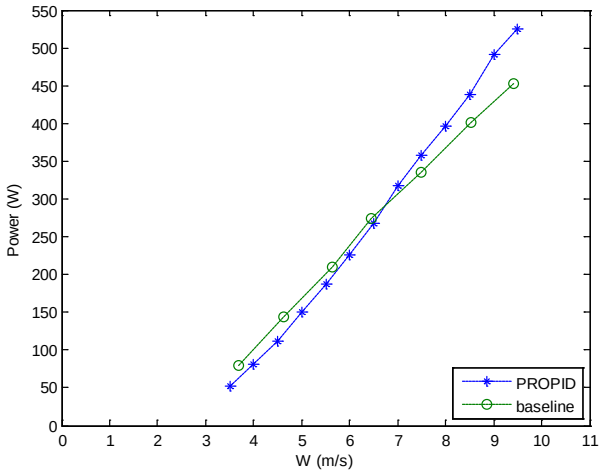

Figure 9. Baseline power measurements compared to PROPID predictions

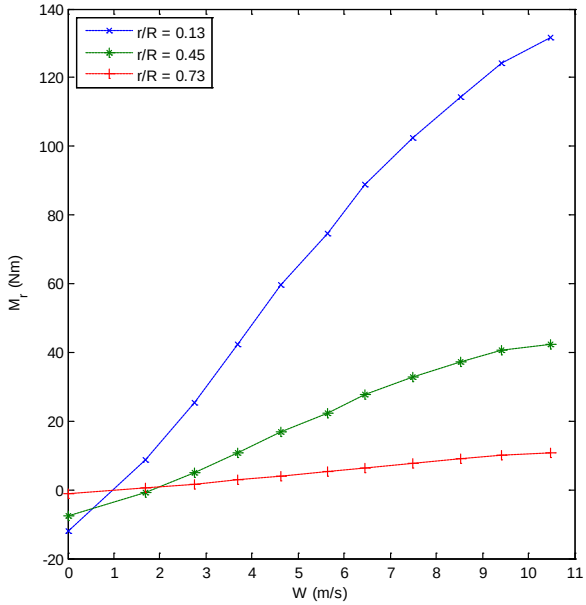

Figure 10. Moment vs. Wind speed measured at each radial position for the baseline case.

4.2. Effect of location and deflection angle of flaps

The first comparison targets the effect of changing the deflection angle of the TEFs on the flapwise bending moment while keeping the location and length constant. The second comparison targets the effect of changing the spanwise location of the TEFs. The F2A formation with sections 4 and 5 (two flaps at 89% and 73% of the blade span) is used to measure the effect of changing the angle. Positive angles represent a deflection towards to pressure side of the airfoil while negative angles represent a deflection towards the suction side.

Measured moments at each strain gage location with the flap activated at 5° and -5°are shown in Figure 11. Since, positive deflection angles increase the C_l of the airfoil section while negative angles decrease the C_l as discussed earlier, the increase and decrease in flapwise bending moment were expected. However, the plots showed no indication of stall occurring, even at higher angles. This is due to the blade operating at lower α towards the tip since the chord and twist were not optimized along the span for this blade. A comparison of the moments of all single flap formations is shown in Figure 12. The deflection angle was set to -15° in all cases. The reduction in moment compared to the baseline case is greatest when the flap was located closest to the tip.

4.3. Effect of changing the flap angle

A comparison of the percentage change of power and moment for the F2A formation at the design speed and for the full range of flap angles is given in Figure 13. The moment at SG1 (blade root) was selected to represent the total change for the full-blade. The plot shows an increase in power with positive deflection angles. An increase in power due to higher C_l was possible without leading to stall as result of the blade twist not being optimized. Positive power augmentation can be useful for wind turbines in low wind conditions allowing operation at higher efficiency by increasing C_l. The increase in power is, of course, accompanied by an increase in the bending moment at a higher rate.

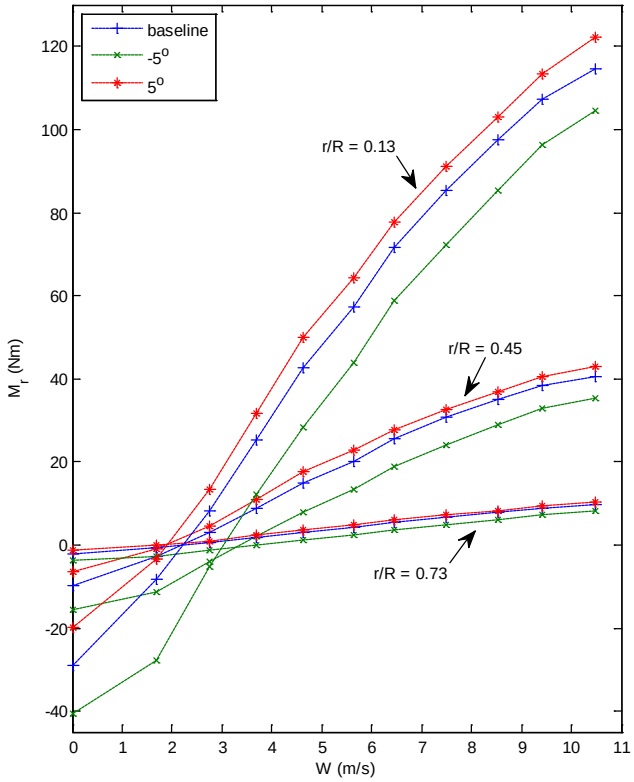

Figure 11. Moment (M_r) vs. Wind speed (W) with the F2A activated at -5° and 5° measured at each radial location.

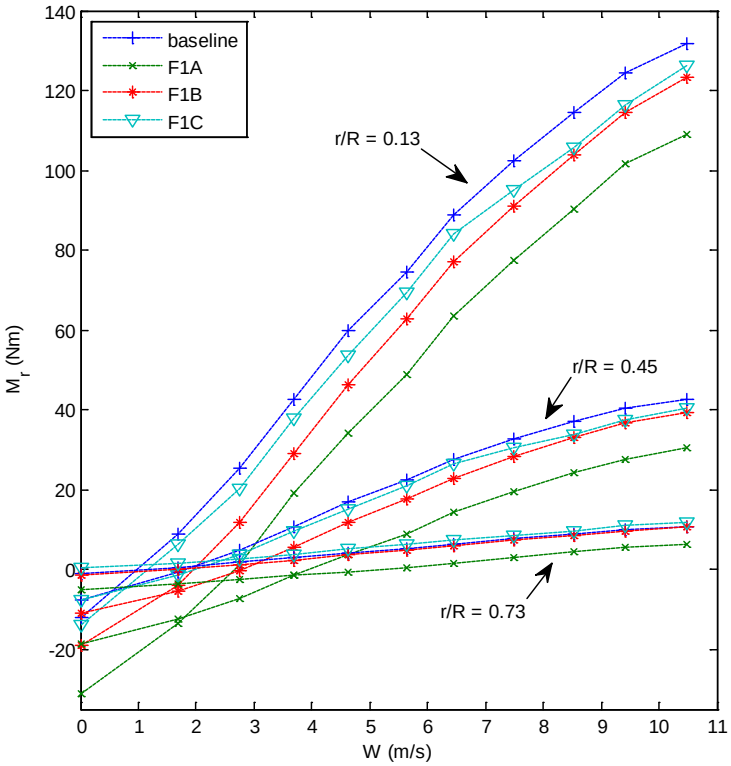

Figure 12. Moment (M_r) vs. Wind speed (W) with the single flap formations (F1X) activated at -15° measured at each radial location.

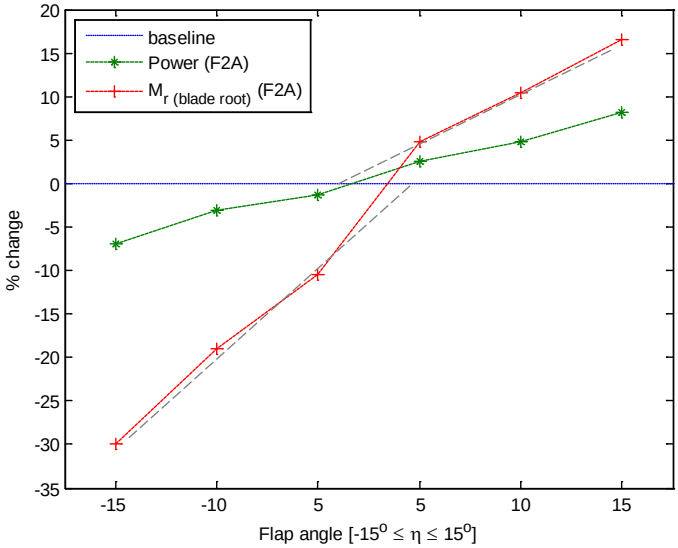

Figure 13. Power and strain reduction (SG1) for the F2A formation (73% and 89% flaps together) at 8.5 m/s.

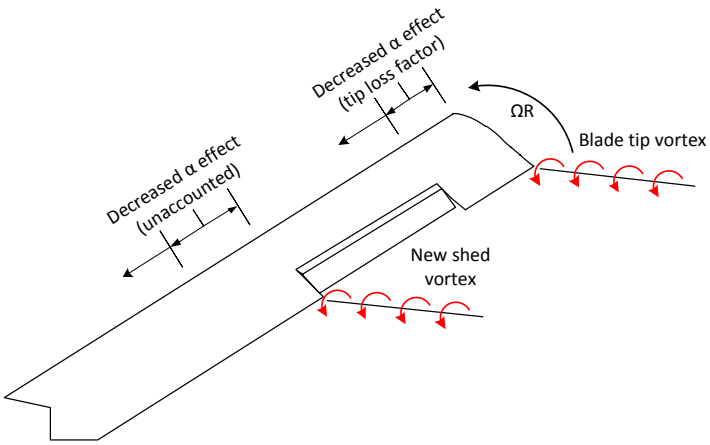

Figure 14. Flap generated shed vortex.

It is evident that the change in moment and power are almost linear. This was expected as indicated by equation 2 derived from thin airfoil theory which indicates a linear relationship between C_l and η. However there is a discontinuity in the gradient between positive and negative deflection angles. This

suggests that the change in blade loading could be affected by other phenomena in addition to the change in the flapped section's C_l.

Another phenomenon that could be possibly causing the decrease in the moment is the formation of strong shed vortices at the newly formed flap tips as shown in Figure 14 as was also noted in [18]. The vortices are similar to the tip vortex created at the end of the blade that induces a decrease in α on the inboard (towards hub) segments of the blade. Loss factor corrections were developed to account for the effect of the tip shed vortex on the tip and inboard sections of the blade. The development of a shed vortex at the newly formed tip where the flap separates from the blade implies that the inboard segments of the blade experience a decrease in lift regardless of flap angle (positive or negative). The decrease in lift for the inboard segments could explain the lower rate of increase of the flapwise bending moment measured for positive deflection angles. The extent of this effect will be the focus of a future investigation.

5. **Conclusion**

An experiment was designed to measure the effect of TEFs on flapwise bending moment and power production of a modular wind turbine blade fabricated using 3D printing. As an initial test, the effects of stationary TEFs were tested for different spanwise locations and deflection angles. The relationship between the flap location and flapwise bending moment was not linear. The total loading on the blade showed significantly higher reduction for the flap placed at 89% of the blade compared to 73% and 56%. For a fixed TEF position, positive deflection angles showed an increase in moment in general, while a negative deflection showed a decrease in moment as expected. The rate of moment change as a function of the deflection angle was linear as expected from theory, however, it was lower for positive deflection. Overall, the experimental set-up proved to be effective in measuring small changes in strain within the wind turbine blade.

6. **Future Work**

The success of the static angle testing of the modular blade flaps and the proven ability of the system to measure moment changes within the blade with high precision and sensitivity introduces numerous possibilities for further research.

Stationary Flap Testing. The experimental setup can utilize a previously developed experimental BEM analysis method in Johnson *et al.* [19] for analysis of the aerodynamic changes caused by TEFs. Such measurements would enable accurate identification of the effects of described phenomena such as the shed vortices created by the TEF configuration. It will also allow the determination of the induction factors for correct computation of α. This method can only be applied for stationary flaps. However, it would prove useful for measurement of changes in C_l and C_d for flapped airfoils for comparison with stationary airfoil wind tunnel experiments and computational codes such as XFOIL [20].

Dynamic Flap Testing. Experimental dynamic testing of TEFs in an active flow control setting can be achieved with the current setup. Similar dynamic studies reported great potential for fatigue load reduction using TEFs as discussed in the Introduction. This would require the addition of a servomotor that can control flap angle adjustment and controller, already part of the design.

Acknowledgments

The authors wish to acknowledge support from the Natural Sciences and Engineering Research Council of Canada and the Ontario Centers of Excellence and thank Curtis Knischewsky at the University of Waterloo for contributions to this study.

References

[1] Barlas T K and Van Kuik G A M 2010 Review of state of the art in smart rotor control research for wind turbines *Prog. Aerosp. Sci.* **46** 1–27
[2] Van Wingerden J W, Hulskamp A. W, Barlas T, Marrant B, Van Kuik G A M, Molenaar D-P and Verhaegen M 2008 On the Proof of Concept of a "Smart" Wind Turbine Rotor Blade for Load Alleviation *Wind Energy* **11** 265–80
[3] Abbott I H and von Doenhoff A E 1959 *Theory of Wing Sections - Including a Summary of Airfoil Data* (Dover Publications)
[4] Burton T, Sharpe D, Jenkins N and Bossanyi E 2001 *Wind Energy Handbook* (John Wiley & Sons)
[5] Bossanyi E A 2005 Further load reductions with individual pitch control *Wind Energy* **8** 481–5
[6] Larsen T J, Madsen HA. and Thomsen K 2005 Active load reduction using individual pitch, based on local blade flow measurements *Wind Energy* **8** 67–80
[7] Lackner M A and Van Kuik G 2009 A comparison of smart rotor control approaches using trailing edge flaps and individual pitch control *Wind Energy* **13** 117–34
[8] Jonkman J, Butterfield S and Musial W 2009 *Definition of a 5-MW Reference Wind Turbine for Offshore System Development* (National Renewable Energy Laboratory)
[9] Andersen P B, Henriksen L, Gaunaa M, Bak C and Buhl T 2010 Deformable trailing edge flaps for modern megawatt wind turbine controllers using strain gauge sensors *Wind Energy* **13** 193–206
[10] Hulskamp A W, Wingerden J W Van, Barlas T, Champliaud H, Van Kuik G A M, Bersee H E N and Verhaegen M 2011 Design of a scaled wind turbine with a smart rotor for dynamic load control experiments *Wind Energy* **14** 339–54
[11] Anderson J D J 2011 *Fundamentals of Aerodynamics* (New York: McGraw-Hill)
[12] Houghton E L and Carpenter P W 1993 *Aerodynamics for Engineering Students* (New York: Wiley & Sons)
[13] Devaud C B, Weisinger J, Johnson D A and Weckman E J 2009 Experimental and numerical characterization of the flowfield in the large-scale UW live fire research facility *Int. J. Numer. Meth. Fluids* **60** 539–64
[14] Gaunt B and Johnson D A 2012 Wind turbine performance in controlled conditions: Experimental results *Int. J. Green Energy*
[15] Gertz D 2011 *An Evaluation Testbed for Alternative Wind Turbine Blade Tip Designs* (Master Thesis, University of Waterloo)
[16] Somers D M 2005 *The S833, S834 and S835 Airfoils* (Technical Report NREL/SR- 500-36340, National Renewable Energy Laboratory)
[17] UIUC Applied Aerodynamics Group PROPID
[18] Miller S L, Quandt G A and Huang S 1998 *Atmospheric Tests of Trailing-Edge Aerodynamic Devices* (NREL/SR-500-22350, National Renewable Energy Laboratory)
[19] Johnson D A, Abdelrahman A and Gertz D 2012 Experimental Indirect Determination of Wind Turbine Performance and Blade Element Theory Parameters in Controlled Conditions *Wind Eng.* **36** 716–37
[20] Drela M 1989 XFOIL: An Analysis and Design System for Low Reynolds Number Airfoils *Low Reynolds Number Aerodynamics* ed T J Mueller (Berlin: Springer-Verlag) pp 1–12